01 Dec 1989

Structural Characteristics Of Sr1-xLaxTi 3+δ As A Function Of Oxygen Partial Pressure At 1400°C

S. A. Howard

J. K. Yau

Harlan U. Anderson
Missouri University of Science and Technology, harlanua@mst.edu

Journal of Applied Physics

RESEARCH ARTICLE | FEBRUARY 15 1989

Structural characteristics of $Sr_{1-x}La_xTi_{3+\delta}$ as a function of oxygen partial pressure at 1400 °C

S. A. Howard; J. K. Yau; H. U. Anderson

Journal of Applied Physics 65, 1492–1498 (1989)
https://doi.org/10.1063/1.342963

Structural characteristics of $Sr_{1-x}La_xTi_{3+\delta}$ as a function of oxygen partial pressure at 1400 °C

S. A. Howard, J. K. Yau, and H. U. Anderson
Department of Ceramic Engineering, University of Missouri-Rolla, Rolla, Missouri 65401

(Received 22 June 1988; accepted for publication 17 October 1988)

The structural characteristics of $Sr_{1-x}La_xTiO_{3+\delta}$ ($0 \leqslant x \leqslant 0.4$) at 1400 °C have been investigated as a function of ambient oxygen partial pressure. A modified Rietveld pattern-fitting structure-refinement program [H. M. Rietveld, J. Appl. Crystallogr. 2, 65 (1969)] was used to determine the nature of the distortions of the fundamental perovskite unit cell, the degree of lattice perfection, and the cation vacancy concentrations. Specimens equilibrated in forming gas displayed a linear relation between x, the lattice parameters, and the degree of lattice perfection while those samples annealed in air and oxygen deviated significantly from linearity. A monoclinic distortion of the perovskite structure was seen in the samples at low oxygen partial pressures while a second phase or layer type of distortion appeared in samples with $x > 0.2$ under oxidizing conditions.

I. INTRODUCTION

$SrTiO_3$ belongs to the class of ABO_3 perovskite compounds ideally having lattices with cubic symmetry but well known for their exhibition of structural distortions. These distortions may arise from the mismatch between ion and crystallographic site size,[1-3] distortion of the oxygen octahedra,[4-6] or cation and/or anion sublattice vacancies.[1,7] The most common pseudocubic lattices are orthorhombic and rhombohedral, but hexagonal and monoclinic lattices are also found with some frequency. Prediction of the lattice symmetry is typically based on the Goldschmidt tolerance factor t, but these distortions are difficult to predict, particularly when partial covalent bonding is present in the compound.[1] Roth[2] has indicated that the polarizability of the ions should also be taken into account in predicting the lattice type. Glazer[8] has systematically evaluated the possible crystallographic distortions based on the various modes of rotation of rigid oxygen octahedra and indicates the expected space groups and relative pseudocubic cell parameters.

In the $SrTiO_3$ system investigated here, the excess charge introduced by the substitution of La^{3+} for Sr^{2+} can be compensated either by an increase in the oxygen content, $(Sr_{1-x},La_x)TiO_{3+x/2}$, or by electronic charge compensation through a change in valence, $(Sr_{1-x},La_x)(Ti^{4+}_{1-x}, Ti^{3+}_{x})O_3$. Studies by Eror and Smyth[9] and Flandemeyer *et al.*[10] have shown that $Sr_{1-x}La_xTiO_{3+\delta}$ demonstrates reversible oxidation-reduction behavior and, hence, charge compensation by change of Ti ion valence.

A structural defect model had to be assumed in order to carry out the Rietveld[11] structure refinement. The two defect models considered were (1) vacancies on the A and/or B cation sublattices or (2) interstitial oxygen on low electrostatic potential sites. Since interstitial oxygen is not common in perovskite structures, we focused our efforts on determining the extent of point defects in the system. Vacancies on the A sites are preferred over B site vacancies due to the low electrostatic potential of the A site. While octahedral B site vacancies are relatively rare in perovskite systems, Hennings and Rosenstein[12] have concluded that the perovskite phases found in the $PbO\text{-}TiO_2\text{-}LaO_{1.5}$ system would form B site vacancies. Tilley[13] suggests that phases having a high static-dielectric constant support changes in stoichiometry not by the creation of point defects but rather by forming planar faults or intergrowths.

Tofield and Scott[4] scrutinized several defect models in their investigation of the perovskite lanthanum manganite system using the Rietveld technique. The authors indicated that better results were obtained by constraining the A and B site vacancies to be equal rather than allowing for only A site vacancies. While their best results were obtained by fixing the B site vacancies at 2% and allowing the A site vacancy concentration to vary, they constrained the A and B site vacancies to be equal. In the present study, we also assumed vacancies on both the A and B sites, an assumption that becomes increasingly valid as the defect concentration escalates. Due to the mathematics involved in the Rietveld refinement, we were required to assume the existence of a complete oxygen sublattice which would not be expected when the cation defect concentration is large. However, the low x-ray scattering ability of oxygen precluded the refinement of the oxygen site occupancies; refinement of x-ray data typically results in large values for the estimated standard deviations of oxygen site occupancies.

The x-ray patterns collected in this study were analyzed with the Rietveld program of Young and Wiles[14] modified by Howard and Snyder[15] to separate the instrumental and specimen contributions to the broadening of the diffraction line profiles. This algorithm has been successfully applied by Yau and Howard[16] to Al and Si systems and has shown to be a powerful method for the analysis of strain in the lattice. Prior to the use of this algorithm, the measurement and profile fitting of diffraction lines from defect-free specimens was required. Calibration curves produced from the refined line parameters are used to calculate the instrumental contributions at any angle. A specimen-related profile function is convoluted with the instrumental contributions and the integral breadth β of the specimen profile is adjusted until the error between the calculated and observed lines is mini-

 0021-8979/89/041492-07$02.40

mized. The value of β for each line may be used to determine the size and strain in the specimen. Crystallite size broadening is constrained to follow:

$$\beta_\tau = \lambda / \tau \cos \theta_k, \quad (1)$$

where τ is the crystallite size and θ_k is the Bragg diffraction angle for the line. Broadening due to strain was modeled by

$$\beta_\epsilon = 4.0\epsilon \tan \theta_k, \quad (2)$$

where the strain $\epsilon = \Delta d / d$. When both size and strain contributions are active, the breadth of the specimen profile is constrained to follow $\beta = \beta_\tau + \beta_\epsilon$.

This separation of the specimen contributions allowed us to quantify specimen defects on an absolute basis. In addition to allowing for crystallite size and strain analysis, the convolute profile generated by this algorithm fits the observed profiles more closely than the traditional profile models employed. The better profile fit allows for better estimates of atom parameters including the thermal and positional parameters. This algorithm also employs a calibration curve to compensate for the angular error of the instrument thus allowing for more accurate determination of the lattice parameters.

II. EXPERIMENT

A. Specimen preparation

The compositions were prepared using a liquid-mix technique[17] to ensure control of stoichiometry and to maximize homogeneous mixing at the atomic level. Each composition was calcined at 800 °C in air for 8 h, divided into three parts and pressed into bars. One bar from each composition was simultaneously placed into a tube furnace through which flowed either pure oxygen, air, or forming gas (90% N_2 + 10% H_2). The bars were annealed at 1400 °C for 17 h before being pulled to the cold end of the tube while the gas flow around the bars was maintained. The parameter matrix and designations of the samples are given in Table I. The physical characteristics after the annealing of the samples are listed in Table II.

The annealed bars were ground with a mortar and pestle and passed through a 400 mesh sieve (30 μm nominal opening size). X-ray data were collected using an automated Scintag PAD V powder diffractometer. Each pattern was collected throughout an angular range of 20°–120° 2θ with an angular increment of 0.02° and a 2-s count time per step. These data were transferred to an IBM 4381 mainframe computer for subsequent processing.

TABLE I. Sample designation in terms of composition and annealing atmospheres for the $Sr_{1-x}La_xTiO_{3+\delta}$ specimens.

	x				
Atmosphere	0.0	0.1	0.2	0.3	0.4
Forming gas	10F	9F	8F	7F	6F
Air	10A	9A	8A	7A	6A
Oxygen	10X	9X	8X	7X	6X

TABLE II. Physical characteristics and cubic lattice parameters of the La-substituted $SrTiO_3$ specimens.

Sample	Color	Crystal system	Lattice parameter (Å)
10F	Gray	Cubic	3.9050
9F	Dark gray	Cubic	3.9111
8F	Black	Pseudocubic	3.9148
7F	Black	Pseudocubic	3.9187
6F	Shiny black	Pseudocubic	3.9056
10A	Brown	Cubic	3.9048
9A	Yellow	Cubic	3.9061
8A	Yellow	Cubic	3.9072
7A	White yellow	Cubic	3.9082
6A	White yellow	Cubic	3.9090
10X	Light brown	Cubic	3.9046
9X	Light yellow	Cubic	3.9061
8X	Light yellow	Cubic	3.9070
7X	White yellow	Cubic	3.9077
6X	White yellow	Cubic	3.9081

B. Determination of crystal system

The initial crystal structure refinement was performed using the cubic space group $Pm3m$ (221) with atom positions corresponding to the ideal perovskite unit. The specimens annealed in air and oxygen showed line broadening that increased as the amount of La substitution increased. Figure 1 shows the results of fitting the patterns obtained from the specimens with the Rietveld program using the cubic $Pm3m$ space group. Figure 1(a) illustrates how the relatively sharp profile of the (200) line in the pure specimen broadened as the lanthanum concentration increased for the series of specimens annealed in oxygen. Figure 1(b) shows

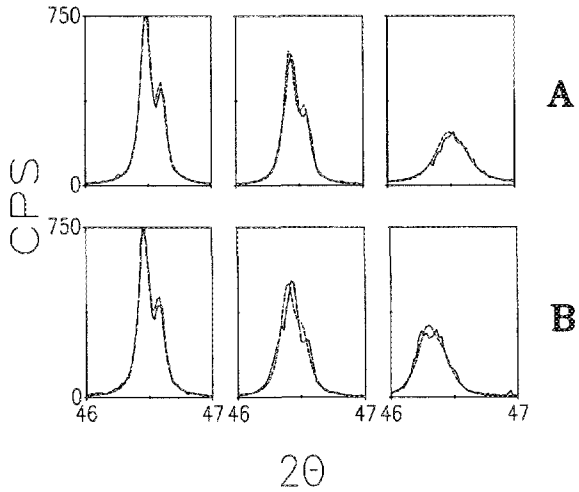

FIG. 1. The distortion of the (200) diffraction line from the $Sr_{1-x}La_xTiO_3$ specimens as a function of La content where $x = 0.0$, 0.2, and 0.4 moving left to right across the figure. The dotted lines are the result of using a single $K\alpha$ doublet to fit the diffraction line. (a) The line broadening observed in the specimens annealed in O_2. (b) The line splitting observed in the specimens annealed in forming gas.

the results obtained in fitting the diffraction lines from the specimens annealed in forming gas. As the lanthanum concentration increased in the reduced specimens, the (200) line broadened and showed signs of splitting reminiscent of a change in crystal system.

The refined cubic lattice parameters for all the specimens are given in Table II and the trends are shown in Fig. 2. The lattice parameters are seen to increase uniformly as a function of x regardless of the atmosphere in which the specimens were annealed. The lattice parameter for those specimens annealed in forming gas showed the greatest dependence on the La content. Since the specimens annealed in forming gas with larger La contents showed structural distortions their lattice parameters should be regarded as pseudocubic values. The specimens annealed in air and oxygen showed monotonically increasing lattice parameters with increasing La content but with a diminishing rate of increase.

In order to determine the crystal structure of the specimens annealed in forming gas, a pseudocell having edge lengths equal to twice the primitive cubic cell edge lengths was utilized in the initial refinement process. This technique allowed for changes from cubic symmetry which would result in tetragonal, orthorhombic, and monoclinic distortions. Symmetry constraints in effect during the structure refinement process forced the trial structures into the *Pmmm*, *P*4*mm*, and *A* 2*m* space groups which would be expected based on systematic rotation of the oxygen octahedra.[8] Results from these refinements indicated that the space group *A* 2*m* yielded the best results. The quality of fit obtained using the *A* 2*m* space group is illustrated in Fig. 3. The refined lattice parameters for the monoclinic specimens are given in Table III.

Distortions were evident in the diffraction patterns obtained from the oxidized specimens which could not be attributed to a change in crystal system. Those specimens having larger values of x exhibited artifacts close to the background level in the 21°–22° and 27°–32° ranges. The artifacts present in the pattern of specimen 6X are shown in Fig. 4. The diffuseness of the lines and their relatively small number precluded identification of any specific phase.

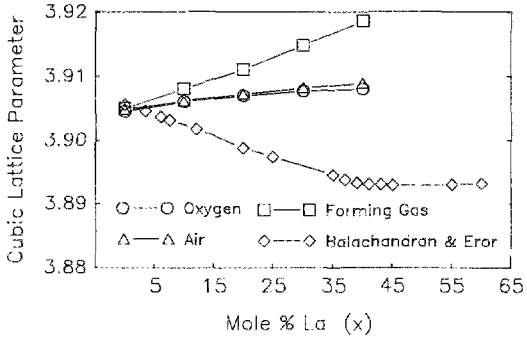

FIG. 2. The refined cubic lattice parameters of the specimens as a function of La content and annealing atmosphere. The values for the reduced $Sr_{0.7}La_{0.3}TiO_3$ and $Sr_{0.6}La_{0.4}TiO_3$ specimens are pseudocubic values since their actual structure is monoclinic.

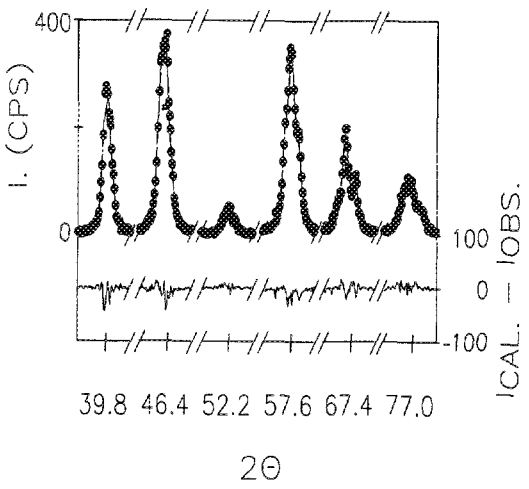

FIG. 3. The good quality of fit to the reduced $Sr_{0.7}La_{0.3}TiO_3$ pattern based on the refined *A* 2*m* monoclinic space group is clearly shown in these results.

C. Structure refinement

The structure related parameters varied during the refinements included the cation site occupancies and the isotropic thermal parameters for the cations. Following Tofield and Scott,[4] we constrained the adjustments in the *A* and *B* site occupancies to be the same during refinement. The atom positions were constrained to those corresponding to the cubic system: the lattice was assumed to simply tilt according to the tilting of the oxygen octahedra. A fourth-order polynomial was used to approximate the background and a coefficient related to specimen displacement was refined in addition to the lattice parameters for the phase. The angular dependence of the specimen profile function was constrained to follow the relationship $\beta = \beta_\tau + \beta_\epsilon$ thus allowing for small crystallite size and strain broadening simultaneously. However, the contributions due to size broadening were so small in all the specimens that the size term was dropped from the refinement.

Table IV lists the refined values of the thermal parameters for each of the specimens. Figure 5 shows the dependence of both the *A* and *B* site occupancies on the La content and annealing atmosphere. The site occupancies were obtained from the refinement of the structure using their previously determined space groups. Again, the trend demonstrated by the specimens annealed in forming gas differed from those specimens annealed in the oxidizing environments. The site occupancies remained nearly constant for the specimens annealed in forming gas whereas the occupan-

TABLE III. Refined lattice parameters for the specimens having monoclinic symmetry.

Sample	*a*	*b*	*c*	*β*
6F	7.847	7.823	7.841	90.19
7F	7.831	7.820	7.838	89.87

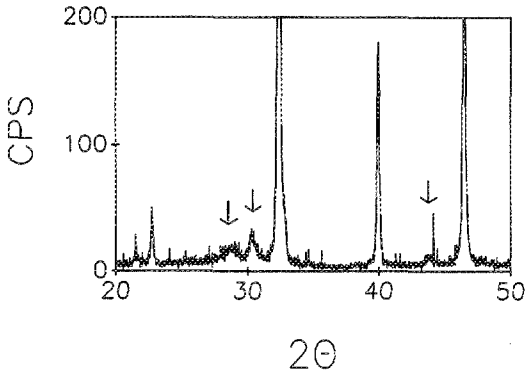

FIG. 4. Artifacts lying close to the background were found in the patterns obtained from specimens annealed in oxygen and air. These artifacts were more evident in specimens with larger La contents. The pattern shown was taken from the $Sr_{0.6}La_{0.4}TiO_3$ specimen annealed in oxygen.

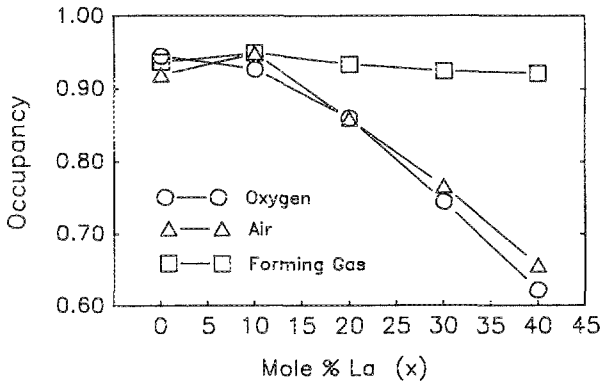

FIG. 5. The fractional occupancies of the A and B cation sites as a function of La substitution and annealing atmosphere. Both site occupancies were constrained to be equal during the structure refinement.

cies for the others varied approximately linearly with x for $x \geqslant 0.10$.

The refined values for the strain in the specimens is shown graphically in Fig. 6. The strain in the specimens annealed in the oxidizing atmospheres apparently goes through a minimum at $x \approx 0.10$ and then begins to increase rapidly. The rapid increase in strain when the value of x exceeds 0.30 coincides with the appearance of the artifacts in the background. The specimens annealed in forming gas showed a nearly linear dependence of the strain on the La content.

III. DISCUSSION OF RESULTS

A. Structural characterization of the reduced specimens

At 1400 °C, the forming gas used in this study ($\approx 10\%$ H_2 in N_2) had an estimated oxygen activity of 10^{-17} atm. Thus, all the specimens annealed in the forming gas were expected to be completely reduced, i.e., their oxygen content was at a minimum.[18] The charge compensation mechanism activated in response to the introduction of the La^{3+} ion into the reduced systems would be assumed to be electronic, i.e., $Ti^{4+} \rightarrow Ti^{3+}$. The alternative charge compensation mechanism, the uptake of oxygen and creation of cation site vacancies, would not be possible since the low oxygen activity would have precluded the expansion of the oxygen lattice.

The results obtained from the analyses of the specimens annealed in forming gas support the electronic charge compensation hypothesis at low oxygen activities. The values of the cation site occupancies, Fig. 5, are virtually constant for all reduced specimens, regardless of the degree of La substitution. The value of the cation site occupancy factor is the same for all specimens and is independent of oxygen activity when the value of x is 0.0. This reflects the fact that there is no compensation mechanism to equalize the charge imbalance that would occur as a result of the loss of oxygen.

The nearly linear dependence of the strain and pseudocubic lattice parameter on x was also consistent with the hypothesis that the La substitution did not result in the creation of cation defects in the reduced systems. The creation of cation defects would be expected to lead to interplanar d

TABLE IV. Refined thermal parameters from the La-doped $SrTiO_3$ specimens obtained via the Rietveld program.

Sample	Sr	Ti	O	
	Isotropic		β_{11}	β_{22}
10F	0.3094	0.1008	0.0215	0.0149
10A	0.3426	0.1821	0.0569	0.0168
10X	0.3350	0.1786	0.0546	0.0102
9F	0.3621	0.1270	0.0121	0.0176
9A	0.4502	0.1247	0.0238	0.0141
9X	0.4348	0.1909	0.0514	0.0166
8F	0.5989	0.3782	0.0534	0.0263
8A	0.6609	0.3116	0.0950	0.0290
8X	0.7419	0.3575	0.0918	0.0258
7F	0.5931	0.3258	0.0515	0.0316
7A	0.8084	0.3196	0.1718	0.0421
7X	0.7281	0.1155	0.1941	0.0407
6F	0.5475	0.2306	0.0370	0.0351
6A	1.0652	0.3126	0.3250	0.0669
6X	0.9715	0.1408	0.3797	0.0715

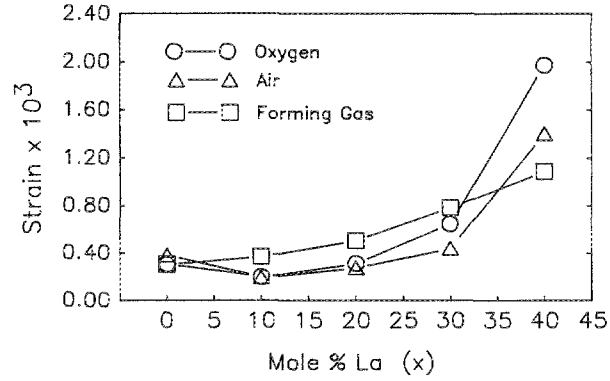

FIG. 6. The dependence of the strain in the specimens on the annealing atmosphere and La concentration.

spacings with less regularity since the ions in the vicinity of vacancies would probably tend to relax. Such irregularity in the d spacings manifests itself through diffraction line broadening and, in this study, would be interpreted as strain. Thus, the observed, nearly linear dependence of the strain on the amount of La substitution is intuitively acceptable. The linear dependance of the pseudocubic lattice parameter simply follows Vegard's law which states that the lattice parameters in a solid solution will vary linearly with composition between the two end members.

In a previous study[19] of $Ba_{1-x}La_xTiO_3$ specimens annealed in flowing H_2, the lattice parameters were observed to decrease as the value of x increased for x up to 0.85. (The lattice parameters of $BaTiO_3$, pseudocubic $LaTiO_3$, and $SrTiO_3$ are 4.02, 3.957, and 3.905 Å, respectively.) Since $Sr_{1-x}La_xTiO_3$ is a member of the solid solution series formed between $LaTiO_3$ and $SrTiO_3$, extrapolation of the lattice parameters from our reduced specimens would be expected to yield an end-point value close to that expected for the pseudocubic $LaTiO_3$. Figure 7 is a comparison of the extrapolated lattice parameters based on our reduced specimens and those from the study by Johnston and Sestrich. The lattice parameters taken from the latter study are half of the true value so the effects of the defect ordering could be canceled. In addition, only the three points in the middle of the composition region were used in the extrapolation since the authors indicated there was a deviation from cubic symmetry outside of this region. Our results are contrary to those obtained in a previous study by Eror and Balachandran[20] where the lattice parameters were reported to decrease as the value of x increased.

B. Structural characterization of the oxidized specimens

According to the defect chemistry in the oxidized systems, one would expect the number of cation defects to be linearly dependent on x. This trend seems to be verified by the cation site occupancy factors as shown in Fig. 5. However, this linear relationship did not manifest itself until the value of x was approximately 0.10. This slow development in the reduction of the cation site occupancies was accompanied by a decreasing strain value which reached a minimum for $x \approx 0.10$. Evidently, the introduction of the La ions allowed the lattice to relax and lower the apparent strain. As the value of x increased beyond 0.10, the strain appears to increase and the cation site occupancies decrease. The fact that the cation site occupancies are not observed to decrease at $x = 0.10$, particularly since the reduction in the occupancy values for $x > 0.10$ is so evident, remains an enigma. Constraining the A and B site occupancies to take the same value may have influenced the result: one of the site occupancies may have dropped, e.g., the Sr site, but its correlation with the Ti site occupancies acted to keep the overall site occupancies relatively constant. The alternative would be a change in the valence of the Ti ion, i.e., $Ti^{4+} \rightarrow Ti^{3+}$, to compensate for the added charge carried by the La^{3+} ion.

In the range of $0.10 \leqslant x \leqslant 0.40$, the cation site occupancies dropped from approximately 95% to 65%. If the occupancies are interpreted on an absolute scale then one may be led to conclude that one cation vacancy was created for each La ion introduced into the system. To create a cation vacancy on both the A and B sites, three oxygen atoms are required to extend the lattice the equivalent of one unit cell. Based solely on ionic charge compensation, six La^{3+} ions would be necessary to cause the uptake of enough oxygen to create the A and B site vacancies. Thus, the expected ratio of La^{3+} ion substitution to vacancy creation should be 6:1 and not the observed 1:1 ratio.

The observed decrease in the cation site occupancies cannot be explained in a straightforward manner. However, we must acknowledge that the refinement model used in our Rietveld analysis was not a literal representation of the problem. The mathematics behind the refinement algorithm would not allow for refining all the occupancy and thermal parameters for the atoms as well as the overall scale factor simultaneously. As stated earlier, we elected to fix the value of the oxygen site occupancies at unity since x rays are not effectively scattered by the oxygen atom. Attempts to manually adjustment the oxygen site occupancies were not effective due to the negligible effect of the perturbations on the residual errors.

There was also a moderate degree of correlation between the site occupancy factors and the Debye–Waller factors for the atoms. A slight decrease in an atom's site occupancy could have been offset by a decrease in its thermal parameter. However, this mechanism could only account for a relatively small uncertainty in either parameter. A larger uncertainty may have been introduced by our use of isotropic rather than anisotropic thermal parameters for the cations. The packing in these perovskites may have allowed atoms on certain sites to have larger vibrational amplitudes in preferred directions[21] which, in turn, may have been manifested in our refinements as a decrease in site occupancies. Due to the limited number of observations (reflections), we were unable to extend the number of variables to include the anisotropic thermal parameters. In addition, the evolution of interlayer phases may have influenced the occupancies and are discussed in the next section.

The thermoelectric power study of $La_xBa_{1-x}TiO_3$ by

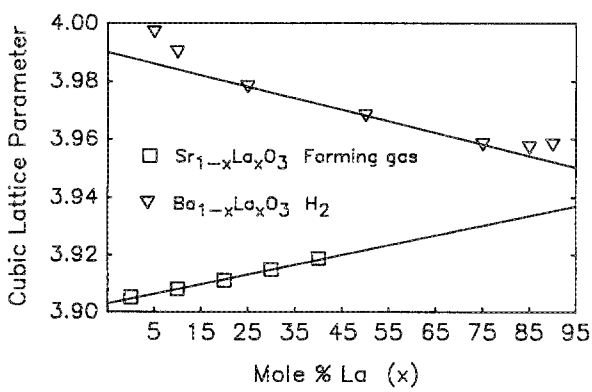

FIG. 7. A comparison of the linear extrapolations based on the lattice parameters obtained from the reduced specimens prepared in this study and those obtained from reduced $La_xBa_{1-x}TiO_3$ by Johnston and Sestrich (see Ref. 19).

Johnston and Sestrich[19] showed that Ti^{3+} was never the stable valence state. When the value of x was close to 1 the compound showed metallic behavior. The authors indicated that the Ti^{3+} ion always tended to become $Ti^{4+} + e^-$ which resulted in good electrical conductivity. Similar characteristics are found in the reduced $Sr_{1-x}La_xTiO_3$ systems. We must then assume that Ti will be found in its most oxidized state and that the oxygen content of the lattice is at its maximum under a given oxygen activity. This, in turn, would tend to drive the cation vacancy concentration to its maximum. If the relatively high cation vacancy concentrations observed in the oxidized specimens were representative of the specimen's true state, we must assume there are oxygen site vacancies in the system in order to maintain charge neutrality. Again, further deliberation of this point is reserved for the discussion regarding structure models below.

The lattice parameters in the oxidized systems were observed to increase and were nearly linearly dependent on x up to $x \approx 0.20$. A close examination of the lattice parameters for specimens with $x > 0.20$ show the rate of increase to diminish. These data, in conjunction with the rapid increase in strain in the systems for $x > 0.30$, may indicate that the Bragg planes are becoming increasingly "puckered" or otherwise distorted. This distortion may have acted to prevent the fullest expansion the unit cell edge lengths and could possibly explain the fact that the lattice parameters from the oxidized specimens were smaller than those from the reduced specimens.

C. The structure of $Sr_{1-x}La_xTiO_3$ annealed in an oxidizing environment

The strain in the oxidized systems increased very rapidly when x exceeded approximately 0.30. This is consistent with the hypothesis that the vacancy concentration in the lattice was increasing rapidly as x increased: the strain would also be expected to increase since the regularity of the Bragg planes would be diminishing. The defects in the oxidized specimens, i.e., the La_{Sr} and V''_{Sr} on the Sr^{2+} sites and the $V_O{\cdot\cdot}$, as well as the strain resulting from these defects, contribute to the overall entropy of the system. Apparently, a limit is reached beyond which it is thermodynamically preferable to (1) precipitate a second phase, (2) cause planar faulting, or (3) promote lamellar intergrowths in the lattice. Both the faulting or intergrowth postulates are consistent with the artifacts found in the x-ray patterns: the artifacts are reminiscent of two-dimensional scattering. The presence of a second phase, even with an extremely fine crystallite size, would have shown more lines: particularly in the concentration necessary to cause the observed artifacts.

In nearly pure $SrTiO_3$, oxygen vacancies are always observed as the defects in either single crystal or ceramic samples.[22-24] In the La-doped $SrTiO_3$ system, Flandermeyer *et al.*,[18] and Eror *et al.*,[25] presented similar models for the reduction and oxidation mechanisms. When samples are annealed in a very reducing environment, only a limited number of $V_O{\cdot\cdot}$ may form and the compensation mechanism for the extra electrons from La^{3+} is the valence change of Ti^{4+} to Ti^{3+}. On the other hand, the samples equilibrated in an oxidizing environment will have ionic compensation, i.e., the creation of cation vacancies, especially V_{Sr}. Between these two extreme states both mechanisms may coexist depending on the oxygen activity. This hypothesis seems to be reinforced by comparing the characteristics of the 10 at. % La-doped and undoped samples. A more perfect anion network would be expected in the first case because of the elimination of oxygen vacancies due to the presence of La^{3+} ions. We observed less strain in the doped case which may be taken to imply that the contributions to strain from the imperfect anion network are greater than the contributions from the cation defects at such low dopant concentrations.

The free Sr resulting from the incorporation of La^{3+} may combine with oxygen to form a layer or two-dimensional structure in the regular $SrTiO_3$ lattice. Ruddleson and Popper[26] and Tilley[13], among others, have investigated the phases found in the SrO-TiO_2 system and have enumerated upon the formation of phases having other than the $SrTiO_3$ stoichiometry. Tilley, has suggested that the lamellae, or ordered intergrowths, may tend to have a composition of $Sr_{n+1}Ti_nO_{3n+1}$ and reported not finding ordered compositions with a value of $n > 2$. The Sr rich phases $Sr_3Ti_2O_7$ and Sr_2TiO_4 have been reported as stable phases at the temperature at which our study was conducted. In particular, $SrTiO_3$ was shown in Tilley's TEM study to show both planar faulting and the intergrowth of the Sr_3TiO_7 phase.

The phases that were considered in attempting to identify the cause of the artifacts in the backgrounds of the patterns from the oxidized specimens are listed in Table V. Based on the positions of their lines and the preference for a Sr-rich phase, the $Sr_3Ti_2O_7$ phase was considered as the prime candidate. The similarity in the structures of $SrTiO_3$ and Sr_3TiO_7, in addition to the intergrowth of the latter phase in the former, may have influenced the cation occupancy values obtained from the structure refinement. In addition, such an intergrowth may account for the increasing strain found for $x > 0.10$ in our quenched specimens, particularly if the thermal expansion of the phases were dissimilar.

Tilley has suggested that phases with a high static dielectric constant, such as $SrTiO_3$, would accommodate changes in stoichiometry through the formation of planar faults or intergrowths rather than through point defects. However, the lack of point defects in his study may have been influenced by the lack of impurities in his material. An

TABLE V. Phases suspect in causing the artifacts in the patterns from the oxidized specimens.

Compound	Crystal system	Lattice parameters a, b, c(Å) α, β, γ(deg)	2θ values of the three strongest peaks (Cu$K\alpha$)
SrO	Cubic	$a = 5.160$	34.77, 29.98, 50.12
$Sr_3Ti_2O_7$	Tetragonal	$a = 3.90, c = 20.36$	31.61, 32.57, 46.57
$La_2Ti_2O_7$	Monoclinic	$a = 7.80, b = 13.01, c = 5.55, \gamma = 98.60$	29.98, 33.05, 27.70
La_2O_3	Monoclinic	$a = 14.60, b = 3.72, c = 9.28, \beta = 99.85$	30.72, 30.94, 47.34
La_4SrO_7			29.88, 28.79, 29.28
La_2SrO_5			28.70, 29.68, 25.90

unpublished TEM study done by one of the current authors (Anderson) has shown the presence of point defect clustering in $Sr_{1-x}La_xTiO_3$. The presence of point defects is consistent with the observed drop in the cation occupancy values and may have preceded or accompanied the faulting or intergrowths in our La-substituted specimens.

[1]H. L. Yakel, Jr., Acta Crystallogr. **8**, 394 (1955).
[2]R. S. Roth, J. Res. Nat. Bur. Stand. **58**, (1957).
[3]G. H. Jonker and J. H. Van Santen, Physica XVI **3**, 337 (1950).
[4]B. C. Tofield and W. R. Scott, J. Solid State Chem. **10**, 183 (1974).
[5]P. M. Raccah and J. B. Goodenough, Phys. Rev. **155**, 155 (1967).
[6]A. Wold and R. J. Arnott, J. Phys. Chem. Solids **9**, 176 (1959).
[7]G. Blasse, J. Inorg. Nucl. Chem. **27**, 993 (1965).
[8]A. M. Glazer, Acta Crystallogr. A **31**, 756 (1975).
[9]Nicholas G. Eror and D. M. Smyth, in *Chemistry of Extended Defects in Non-Metallic Solids*, edited by Leroy Eyring and Michael O'Keeffe (North-Holland, Amsterdam, 1970), pp. 62–75.
[10]B. K. Flandermeyer, M. M. Nasrallah, D. H. Sparlin, and H. U. Anderson, Physica **129**, B (1985).
[11]H. M. Rietveld, J. Appl. Crystallogr. **2**, 65 (1969).
[12]D. Hennings and G. Rosenstein, Mater. Res. Bull. **7**, 1505 (1972).
[13]R. J. D. Tilley, J. Solid State Chem. **21**, 293 (1977).
[14]R. A. Young and D. B. Wiles, J. Appl. Crystallogr. **15**, 430 (1980).
[15]S. A. Howard and Robert L. Snyder, J. Appl. Crystallogr. (in press).
[16]J. K. Yau and S. A. Howard, J. Appl. Crystallogr. (in press).
[17]Nicholas G. Eror and Harlan U. Anderson, Mater. Res. Symp. Proc. **73**, 571 (1986).
[18]B. F. Flandermeyer, A. K. Agarwal, H. U. Anderson, and M. M. Nasrallah, J. Mater. Sci. **19**, 2593 (1984).
[19]W. D. Johnston and D. Sestrich, J. Inorg. Nucl. Chem. **20**, 32 (1961).
[20]U. Balachandran and N. G. Eror, J. Solid State Chem. **39**, 351 (1981).
[21]F. A. Kassan-Ogly and V. E. Naish, Acta Crystallogr. B **42**, 307 (1986).
[22]U. Balachandran and N. G. Eror, Solid State Sci. Technol. **129**, 5 (May 1982).
[23]H. Yamada and G. R. Miller, J. Solid State Chem. **6**, 169 (1973).
[24]L. C. Walters and R. E. Grace, J. Phys. Chem. Solids **28**, 239 (1967).
[25]N. G. Eror and U. Balachandran, J. Solid State Chem. **40**, 85 (1981).
[26]S. N. Ruddelson and P. Popper, Acta Crystallogr. **11**, 54 (1958).